


X-ray reverberation in 1H 0707–495 revisited

L. Miller¹ , T. J. Turner^{2,3}, J. N. Reeves⁴ and V. Braito⁵

¹*Dept. of Physics, Oxford University, Denys Wilkinson Building, Keble Road, Oxford OX1 3RH, U.K.*

²*Dept. of Physics, University of Maryland Baltimore County, Baltimore, MD 21250, U.S.A.*

³*Astrophysics Science Division, NASA/GSFC, Greenbelt, MD 20771, U.S.A.*

⁴*Astrophysics Group, School of Physical and Geographical Sciences, Keele University, Keele, Staffordshire ST5 8EH, U.K.*

⁵*Dept. of Physics and Astronomy, University of Leicester, Leicester LE1 7RH, U.K.*

23 November 2018

ABSTRACT

The narrow-line Seyfert 1 galaxy 1H 0707–495 has previously been identified as showing time lags between flux variations in the soft- (0.3–1 keV) and medium-energy (1–4 keV) X-ray bands that oscillate between positive and negative values as a function of the frequency of the mode of variation. Here we measure and analyse the lags also between a harder X-ray band (4–7.5 keV) and the soft and medium bands, using existing *XMM-Newton* data, and demonstrate that the entire spectrum of lags, considering both the full energy range, 0.3–7.5 keV, and the full frequency range, $10^{-5} \lesssim \nu \lesssim 10^{-2}$ Hz, are inconsistent with previous claims of arising as reverberation associated with the inner accretion disk. Instead we demonstrate that a simple reverberation model, in which scattering or reflection is present in all X-ray bands, explains the full set of lags without requiring any *ad hoc* explanation for the time lag sign changes. The range of time delays required to explain the observed lags extends up to about 1800 s in the hard band. The results are consistent with reverberation caused by scattering of X-rays passing through an absorbing medium whose opacity decreases with increasing energy and that partially-covers the source. A high covering factor of absorbing and scattering circumnuclear material is inferred.

Key words: galaxies: active - X-rays: galaxies - accretion, accretion disks - galaxies: individual: 1H 0707–495

1 INTRODUCTION

1H 0707–495 ($z = 0.0411$) is a narrow-line Seyfert 1 galaxy, notable for the presence of an unusually deep drop in its X-ray spectrum just above 7 keV (Boller et al. 2002). The spectral drop has been modeled as an edge whose energy varies between observations (Gallo et al. 2004) and the overall spectral form can be explained using partial-covering models (Boller et al. 2002; Tanaka et al. 2004; Gallo et al. 2004). However, Fabian et al. (2004) suggested instead that the spectral drop may be the blue wing of a relativistically-broadened Fe K α emission line. Recently, Fabian et al. (2009, hereafter F09) and Zoghbi et al. (2010, hereafter Z10) have claimed that the soft X-ray spectrum of 1H 0707–495 contains strong, blurred Fe L line emission below 1 keV. F09 and Z10 explain the flux-dependent spectral variability as due to varying contributions from a powerlaw continuum and an ionized reflector with high metallicity. To fit the spectrum, the reflected emission is extremely relativistically redshifted and blurred, with contributions down to 1.23 gravitational radii (GM/c^2) from an illuminated disk with reflected emissivity $\propto r^{-7}$ (where r is the radial coordinate from the black hole). Such a conclusion is surpris-

ing, given the extreme black hole spin, the very steep reflectivity profile required to obtain detectable emission from so close to the black hole, and the implied very small size of illuminating source. However, F09 argue that the combination of this spectral modelling with an analysis of the source’s rapid flux variations does provide evidence for emission from a few tens of light-seconds of the event horizon of a rapidly-spinning black hole, and hence it is important to critically assess that model and test it with further analysis.

In addition to the spectral modelling, F09 and Z10 searched for and detected time lags between flux variations in two X-ray energy bands, 0.3–1 keV and 1–4 keV. Lags were analysed in the Fourier domain, so that they could be derived as a function of the frequency of the mode of flux variation. Those analyses revealed the first clear detection of “negative lags” in the X-ray time series of an active galactic nucleus (AGN), where negative is defined as meaning that flux variations in the softer energy band lag variations in the harder energy band. Negative lags were found at high frequencies ($\nu > 6 \times 10^{-4}$ Hz) of amplitude up to about 40 s. Larger positive lags were found at lower frequencies. Positive lags are well-known in AGN (e.g. McHardy et al. 2004), but a previous detection of a negative lag was not strongly significant (McHardy et al. 2007) and the measurement of both positive and negative lags in an AGN had not been clearly established prior to the work of F09 and Z10. F09/Z10 interpreted the high-

* E-mail: L.Miller@physics.ox.ac.uk

Table 1. Summary of observations used: epoch, observation ID, start date, duration rounded to the nearest ks, and mean 0.3-7.5 keV count rate.

epoch	ID	start date	duration /ks	count rate /s ⁻¹
O2	0148010301	13-10-2002	68	3.841 ± .007
O3	0506200301	14-05-2007	36	2.028 ± .007
O3	0506200401	06-07-2007	17	4.227 ± .016
O3	0506200501	20-06-2007	34	6.116 ± .013
O4	0511580101	29-01-2008	93	3.504 ± .006
O4	0511580201	31-01-2008	68	5.163 ± .009
O4	0511580301	02-02-2008	68	4.509 ± .008
O4	0511580401	04-02-2008	68	3.656 ± .007

frequency negative lags qualitatively as a reverberation signal originating within a gravitational radius of the black hole event horizon, and argued that this interpretation was consistent with their spectral model, with its large component of relativistically-blurred reflected emission in the soft band. Z10 recognised that the larger-amplitude, low-frequency positive lags could not arise from such inner-disk reflection, and therefore suggested that these lags might have an origin other than reverberation. However, Miller et al. (2010) analysed the positive lags in the time series of *Suzaku* X-ray flux variations of NGC 4051, and recognised that the energy- and frequency-dependence of those lags may be well-explained by reverberation from substantially more distant material, a few thousand light-seconds from the illuminating source, leading to the question of whether such a reverberation model is relevant also to 1H 0707–495.

In their timing analysis of 1H 0707–495, F09 and Z10 did not report any measurement of lags for energies above 4 keV, thereby losing the diagnostic potential of measuring a band that contains Fe K emission. This is particularly important given that the F09/Z10 spectral model predicts that an even larger fraction of reflected light should be present in the Fe K spectral region. In this paper we show measurements of the lags at higher energy and investigate both whether the Z10 model can explain the full set of observed lag behaviours and whether a reverberation model such as that inferred for NGC 4051 is able to explain the frequency-dependent positive and negative lags seen in 1H 0707–495.

2 OBSERVATIONS AND DATA REDUCTION

XMM-Newton has observed 1H 0707–495 during four epochs, 2000 Oct (O1), 2002 Oct (O2), 2007 Jan-Feb (O3) and 2008 Jan (O4), where the names in parentheses indicate the naming convention used by Z10. As we might worry that different behaviour arises in low or high flux states, we only consider observations whose flux is comparable to that of the long O4 observations. Thus, in this paper we present the detailed analysis of data from 2002–2008, excluding the first of the 2007 snapshots (see Table 1 and Z10).

The European Photon Imaging Camera (EPIC) observations were made with the medium filter and with the prime full window mode in 2002 and the prime large window mode in 2007/8. Data were processed using SAS v8.0.0 and HEASOFT v6.8. Our analysis used only the pn data, which offered the best S/N ratio of all EPIC data and which were free of pile-up effects. The pn events were filtered using standard criteria and instrument patterns 0–4 were selected. Source events were extracted from circular regions of radius 35'' centred on the source, and background events sampled from regions on the same chip about a factor 5 larger in area than the source cell. The 2007/8 observations suffered from high background, with some background flaring. As noted by Z10,

the high background is problematic owing to prominent emission lines from the electronics circuit board. The geometry of the circuit board results in the cleanest area being the central region of the pn chip array, comprising about the inner 40% of the chip at the nominal aim point (Lumb et al. 2002). However, with the target positioned in the clean area, it is difficult to find a sufficiently large area for similarly clean background extraction on the same pn chip. In order to be able to use the largest possible background extraction area while minimizing contamination by the background emission lines, we applied a tight background screening to the data and removed periods when the full-band pn background count rate exceeded 0.25 count s⁻¹. After screening, the data had a background level < 1% of the source count rate in the 0.3–1 keV and 1–4 keV bands and 10–15% of the source count rate in the 4–7.5 keV band. The total effective pn exposures were 68 ks (O2), 87 ks (O3) and 297 ks (O4). 1H 0707–495 ranged in flux from < 1 count s⁻¹ in the lowest observed states (not analyzed here) to ~ 10 count s⁻¹ in the higher states observed with *XMM-Newton*.

3 TIME LAG MEASUREMENT

F09 and Z10 have previously considered the time lags only between two bands: a “soft” band (0.3–1.0 keV) and a “medium” band (1.0–4.0 keV). We add a further “hard” band covering 4.0–7.5 keV, where the upper energy bound has been chosen to include the Fe K region but avoid the region of greatest residual background contamination.

To measure time lags between these bands we follow the method of Miller et al. (2010), which uses a maximum-likelihood formalism to measure the best-fitting power spectral densities (PSD) in each band and the cross-power spectral densities and time lags between bands. To measure a PSD alone, the PSD is defined as the Fourier transform of the autocorrelation function, $\mathcal{A}(\tau)$, as in other methods, but rather than trying to invert directly the observed autocorrelation function, instead we maximise the likelihood, \mathcal{L} , of the observed $\mathcal{A}(\tau)$,

$$\mathcal{L} = \frac{1}{(2\pi)^{N/2} |C|^{1/2}} \exp \left[-\frac{1}{2} \Delta^T C^{-1} \Delta \right], \quad (1)$$

for a time series containing N data samples, where C is a $N \times N$ model covariance matrix, whose elements are given by the model's $\mathcal{A}(\tau)$, Δ is the time series vector of fractional fluctuations with length N and Δ^T is its transpose. The likelihood function assumes the process that generates the time series to be gaussian (or, equivalently, assumes that the Fourier transform of the intrinsic time series, before being observationally sampled, has uncorrelated phases): in principle this assumption could be varied and replaced by a lognormal distribution, however there is no strong evidence in this time series for non-gaussian behaviour, and the assumption of gaussianity is common to alternative methods of PSD estimation (e.g. Uttley et al. 2002). To find the best-fitting PSD we compute the expected covariance matrix for an initial set of model parameter values and iterate using the method of Bond, Jaffe & Knox (1998). The model covariance matrix includes the effects of shot noise (see Miller et al. 2010). The model parameters are the amplitudes of the PSD in discrete ranges of Fourier frequency (and in the case of estimation of the cross-spectrum for a pair of time series, the model parameters also include the time lags, see below).

The method has the principal advantages over other approaches that it is immune to gaps in the time series data or to uneven time sampling with no need for any interpolation (because

the likelihood function is only defined for the observed time series); it corrects rigorously for the presence of shot noise (including the effect of uncertainty in the shot noise); and it allows rapid estimation of the uncertainties in the PSDs and time lags, including estimation of the covariance between frequency bins. Crucially, although PSD uncertainties are not gaussian, and neighbouring frequencies have correlated errors, because the likelihood is calculated in the time domain the PSD uncertainties and their covariance are straightforward to calculate using either of two methods. First, as part of the likelihood iteration, we calculate the model Fisher matrix (see Bond et al. 1998 for full details) and when the model is a good description of the data, the square-root of the diagonal elements of the inverse Fisher matrix yield an estimate of the uncertainties on the PSD parameters. Strictly, these estimates are lower limits to the true uncertainties (the Cramér-Rao bound) and do not allow for the correlations between parameters which are encoded in the off-diagonal elements of the inverse Fisher matrix. To address these issues we may instead step through a set of values for each parameter and measure the likelihood ratio, $\mathcal{L}/\mathcal{L}_{\max}$, with respect to the best-fitting model, allowing other parameter values to float in the maximisation (a procedure similar to marginalisation over those other parameters). In this case, we expect $\chi^2 = -2 \log(\mathcal{L}/\mathcal{L}_{\max})$ to be distributed as χ^2 with one degree of freedom. Thus 68 percent confidence intervals are found when χ^2 increases by unity. The second method is more time-consuming, of course. The error estimation methods have been tested against Monte-Carlo realisations for the Miller et al. (2010) observation of NGC 4051 by Miller (in preparation) and found to be in excellent agreement with the distributions obtained from those realisations.

To measure time delays between two time series, we follow Miller et al. (2010) and extend the likelihood maximisation to include the cross-spectrum of the pair of time series, by including both time series in the vector Δ in equation 1, so that the maximisation process involves handling matrices of rank $2N$. The time delays are then obtained from the phases of the cross-spectrum (e.g. Nowak et al. 1999).

Although in principle the multiple observations described in Table 1 may be analysed as a single time series, in practice this is computationally time-consuming at high time sampling as it requires the inversion of several $2N \times 2N$ matrices, a process which becomes prohibitively expensive on desktop computers for $2N \gtrsim 6000$. We therefore follow an approach equivalent to that of Z10 in which we ignore the temporal cross-correlation between time samples from different orbits, but combine the likelihoods deduced from each observation to obtain an overall best-fit set of PSD and time lag values.

Time series were generated with 48 s sampling. PSDs were measured for frequency bins of width $\Delta \log_{10} \nu = 0.3$ for frequencies lower than the Nyquist frequency of 0.0104 Hz. The bin widths were increased for the lowest frequency bins to ensure that their widths were at least twice the lowest observable frequency of the longest individual dataset, so that neighbouring frequency bins are largely uncorrelated. Fig. 1 shows the PSD estimates in each of the three energy bands. The vertical error bars show the expected 68 percent confidence intervals expected from the square-root of the diagonal elements of the inverse Fisher matrix, and hence do not allow for covariance between parameters: we do not calculate stepped-likelihood uncertainties as we make no further analysis of the PSDs in this paper. The PSDs are steep above 10^{-4} Hz, although the harder bands have flatter PSDs than the soft band (as found also in other AGN, e.g. NGC 4051, Miller et al. 2010).

Fig. 2 shows the derived time lags as a function of frequency

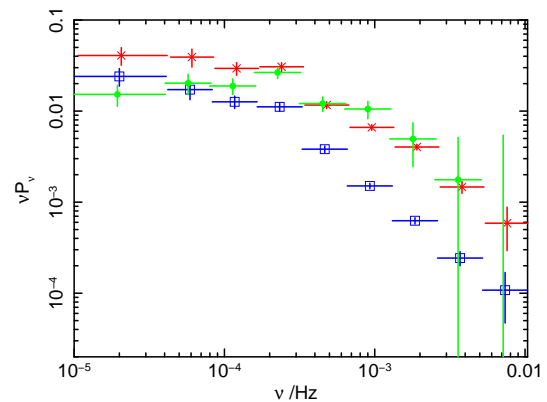


Figure 1. Power spectral densities, νP_ν , as a function of mode frequency ν for each of the three X-ray energy bands: soft (open squares); medium (crosses) and hard (closed circles). Vertical bars indicate 68 percent confidence uncertainty, horizontal bars show the range of frequencies included in each point. Frequency values have been slightly offset between energy bands for clarity.

(the “lag spectrum”). As we now need to sample rapid variations as a function of frequency, a higher frequency resolution, $\Delta \log_{10} \nu = 0.15$, was chosen, which also matches more closely the resolution adopted by Z10. Again, the frequency bin widths were increased to maintain independence at low frequencies. One further bin at lower frequency was included in the maximisation but is not shown in Fig. 2 as its uncertainty is too large to be useful. The 68 percent confidence region uncertainties shown were calculated by measuring the likelihood ratio obtained when stepping through parameter values, as described above, and thus account for the covariance with other parameters and for the non-gaussianity introduced by transforming from the time domain to the Fourier-phase domain. As we have used the combined datasets O2, O3 (high-state) and O4, with rejection of high-background segments, and slightly different sampling from Z10, we do not expect the medium-soft lags to be identical to those of Z10. There is however good general agreement, with maximum positive lags of 237 ± 72 s and maximum negative lags of -32 ± 5 s at higher frequencies. The uncertainties appear similar to those obtained by Z10.

We can see that the hard-soft lags, not reported or discussed by F09 or Z10, follow the same pattern with a larger amplitude of time lag. The maximum positive lag in this case is 548 ± 266 s, with the most statistically-significant individual positive lag being 277 ± 62 s. The most negative lag has a value -55 ± 25 s. The existence of several neighbouring lags with similar values further increases the statistical significance of both the positive and negative lags. The overall significance of the negative lags is discussed further below. The lags measured between medium and hard bands are not independent of the medium-soft and hard-soft lags and are generally in reasonable agreement. There is some disagreement at the highest frequencies owing to degeneracies in the fit, highlighting the difficulty of obtaining a unique measurement at high frequencies.

4 DISCUSSION

4.1 The interpretation of time lag spectra

Before discussing in some detail the explanation of the observed lag spectra, there are some general points to be made.

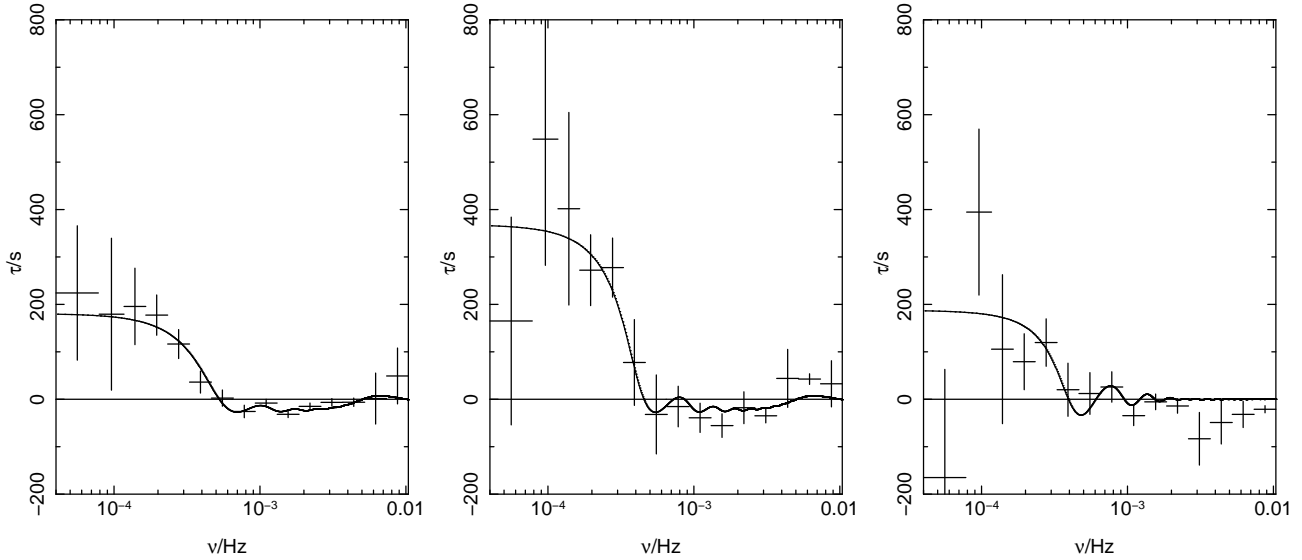


Figure 2. Measured lag spectra (defined to be positive for the harder band lagging the softer band), shown as points with error bars, from the cross-band power spectra of the medium v. soft bands (left panel), hard v. soft bands (centre panel) and hard v. medium bands (right panel). Vertical bars indicate 68 percent confidence regions from the stepped-likelihood method. Horizontal bars indicate the range of frequencies used for each point. Solid curves show the lag spectra expected from top-hat model transfer functions discussed in section 4.3.

(i) It has become common-place in X-ray timing analysis to inspect the time lag spectrum and to consider each measured frequency as being in some sense independent of the others. This approach is flawed in the case where lags are caused by reverberation, because in general we expect any reverberation signal that is restricted to some finite range of time delays to produce lag spectral signals over the full measurable range of frequencies. The most extreme case would be for reverberation seen from a narrow annulus on an accretion disk viewed face-on: in this case the transfer function is a delta-function and its Fourier transform has amplitude and phase information distributed over all frequencies. In the case of the analysis of 1H 0707–495, any claim of a reverberation signal at high frequencies should be accompanied by a demonstration of the expected time lag signatures at all frequencies.

(ii) In reverberation models, the measured lag spectrum is a representation of the phases of the Fourier transform of the transfer function. Low-frequency modes have time lags in the same sense as the reverberation lag (i.e., if the hard band contains more reflected emission than the soft band, the low frequency modes have positive lags) but for modes whose time period is less than the reverberation delay, the phase wraps around: phases are evaluated in the range $-\pi < \phi \leq \pi$ and so any apparent time lag, positive or negative, is possible. A corollary statement is that high-frequency modes cannot generate large apparent time lags (i.e. any inferred time lag at some frequency ν must satisfy $|\tau| < 1/2\nu$) regardless of the actual time delay.

(iii) Because in the X-ray band the signals are likely to be a combination of reflected, time-delayed emission and directly-viewed emission, the measured time delay is always less than the true time delay (i.e. the true time delay is diluted by the addition of the direct emission - see Miller et al. 2010).

(iv) In cross-correlating two bands and measuring the time delays between them, there is likely to be reflected emission in both bands, and thus the inferred transfer function is the cross-correlation of the individual transfer functions of each band.

(v) The existence of small time lags does not necessarily indi-

cate a short light travel-time between the source and the reflector, because reflection from material along the line of sight, at any distance from the source, has zero time delay with respect to directly-viewed emission, and slightly off-axis material can result in arbitrarily small delays. As an example, consider the transfer function of a thin spherical shell of reflection, of radius r , isotropically surrounding a source. The transfer function is a uniform top-hat distribution with time lags $0 \leq \tau \leq 2r/c$ (Peterson 1993): the existence of lags close to zero do not imply that the reflecting material has to be close to the source, and such a conclusion could not be reached unless a full model reproducing the time lags for all modal frequencies were to be tested against the data.

Bearing these points in mind, we shall first critically review the previous analyses of the lag spectra of 1H 0707–495, and then discuss a more viable model that explains all the observed features.

4.2 The inconsistency with inner-disk reflection

The observed time lags are inconsistent with the hypothesis that they arise from reflection from the inner accretion disk, as proposed by F09 and Z10, for a number of reasons. In this section we first discuss the hypothesis of F09/Z10, that there are two independent lag-generating mechanisms that operate at different frequencies, and we then move on to test consistency of the new hard-band lag measurements with the F09/Z10 model.

4.2.1 Constraints on two mechanisms of lag generation

Consider first the time lags discussed by F09 and Z10, between the soft and medium bands. At low frequencies, $\nu \lesssim 10^{-3.5}$ Hz, the medium band lags the soft band, which is inconsistent with the soft band containing delayed reflection of the medium band. The signature of inner-disk reflection is supposed instead to be the small (~ 30 s) negative lags at high frequencies ($\nu \gtrsim 10^{-3}$ Hz).

This was claimed to place the reflecting region a few tens of light-seconds away from the Fe L ionising source, traced by the medium band. But if there are longer-timescale fluctuations in that source, as observed, these must also be delayed in the same sense: i.e. there should be a negative lag of tens of seconds at low frequencies. This is not observed, instead positive lags of ~ 200 s are seen. F09 and Z10 suggested these arise as a separate process, such as the propagation of fluctuations through an accretion disk from outer to inner radii, with the inner disk emission supposedly having a harder powerlaw spectrum than the outer disk, so that the softer band varies sooner than the harder band (Arévalo & Uttley 2006). This scenario could only produce the observed lag spectra if (i) inward radial perturbations leading to variable emission existed and (ii) radial dependence of the spectrum existed and (iii) the softer outer disk regions did not vary on short timescales, whereas the harder inner disk regions did, and (iv) the outer disk emission did not result in any soft-band reflection, implying the outer disk spectrum to be strongly cut off just at the Fe L ionisation edge, and (v) despite having emission from a wide range of radii, nonetheless the reflected emission had a radial r^{-7} dependence (F07, Z10). Such a set of requirements is not necessary if a more straightforward explanation is adopted (section 4.3). These considerations motivate us to carry out further evaluation of the viability of the Z10 model.

4.2.2 Testing the model for consistency with the hard-band lags

The hard band (4–7.5 keV) analysed here also shows significant time lags with respect to the soft band, again in the sense that the hard band lags the soft band by up to ~ 550 s at low frequencies, with negative lags at high frequencies. However, the hard band contains the Fe K region and, in the Z10/F09 model, should also show delays with respect to its ionising continuum. According to the model, most reflection occurs in the hard band, then the soft band, then the medium band with the least (but non-zero) reflection (see Fig. 8 of Z10). We find that the hard-soft lag spectrum has an almost identical form to that of the medium-soft lag spectrum, but with lags of larger amplitude, despite the expectation from the Z10 model that the hard band supposedly has more reflection than the soft band and thus should lag the soft and medium bands at $\nu \gtrsim 10^{-3}$ Hz (i.e. the hard-soft and hard-medium lags should be positive where the medium-soft lags are negative).

We have assessed the statistical significance of the disagreement with the model as follows. Starting with the medium-soft lag spectrum, we find the mean lag of the six frequency bins that have negative lags, i.e. $0.00066 < \nu < 0.0053$ Hz, by fitting a single time lag value to that frequency range and evaluating its uncertainty using the maximum-likelihood method. All other bandpower amplitudes and time lags were allowed to vary during the likelihood maximisation. The 68 percent confidence interval for that one parameter is given by $\Delta\chi^2 = -2\log(\mathcal{L}/\mathcal{L}_{\max}) = 1$, which yields a mean lag $\tau_{\text{medium-soft}} = -16.4 \pm 2.4$ s. The mean lags for the same frequency range in the other comparisons between wavebands are $\tau_{\text{hard-soft}} = -37.0 \pm 9.0$ s and $\tau_{\text{hard-medium}} = -14.7 \pm 8.7$ s (note that these three lag values are not statistically independent but are consistent with each other). Thus all three lag spectra are significantly negative in the frequency range of interest, counter to the expectation of the Z10 model.

To compare with the Z10 spectral model, we estimate the expected relation between the lags in the three bands as follows. In a waveband where both direct and reflected light is present, with reflection fraction f , the inferred lag, τ' , is diluted with respect to the intrinsic time lag to the reverberating region, τ , such that

$\tau' \simeq f\tau/(1+f)$ for $\omega\tau \ll \pi$ when considering Fourier modes with angular frequency ω (Miller et al. 2010). Thus the inferred lag between two such bands, designated i and j , with reverberation signals from the same region, is given by

$$\Delta\tau'_{ij} \simeq \left(\frac{f_i}{1+f_i} - \frac{f_j}{1+f_j} \right) \tau. \quad (2)$$

We obtained values for the reflection fractions f_{soft} , f_{medium} , f_{hard} in each of the soft, medium and hard bands respectively by refitting to the data the model described by Z10, with reflection spectrum given by relativistically-blurred REFLIONX tables (Ross & Fabian 2005)¹. As the time series analysis was carried out on variations in count rate and not flux (as this optimises the signal-to-noise in the timing analysis) the fractions f have been obtained as ratios of counts in the blurred reflection component to the counts in the power-law component in each band. The reflection fractions in the summed observations were $f_{\text{soft}} = 1.60$, $f_{\text{medium}} = 0.57$ and $f_{\text{hard}} = 2.03$ in the soft, medium and hard bands respectively. The formal statistical uncertainties on the model fits are very small, however we expect there to be some possible variation in allowable models, and to allow for this modelling uncertainty we also fitted the Z10 model to the data from each of the four separate orbits that make up the main O4 observation. The sets of four reflection fractions were found to be $f_{\text{soft}} = \{1.63, 1.13, 1.57, 2.48\}$, $f_{\text{medium}} = \{0.58, 0.40, 0.57, 0.91\}$, $f_{\text{hard}} = \{2.04, 1.45, 2.05, 3.58\}$ in each band for each of the observation IDs 0511580101, 0511580201, 0511580301, 0511580401 respectively. Inserting these reflection fractions f into equation 2, we can predict the expected relation between the observed lags in each band for any assumed value of distance of the reflector from the primary source.

Fig. 3 shows these expected relations and contours of $\Delta\chi^2$ obtained from the maximum-likelihood fitting, comparing in turn the hard-soft lags and the hard-medium lags with the medium-soft lags. Confidence region contours are shown at $\Delta\chi^2 = 2.3, 4.6, 9.2, 13.8$ which correspond to the 68, 90, 99, 99.9 percent confidence regions for two parameters. The failure of the hard-soft lags to have the opposite sign to the medium-soft lags rules out the Z10 model at > 99.9 percent confidence. The medium-soft lags also rule out the model at > 99 percent confidence, although these two measures are not independent.

4.3 The reverberation transfer function

We can use the considerations of section 4.1 together with the new information from the hard band to infer what reverberation model could explain the full set of available information. Given that a reverberation explanation should also seek to explain the large positive lags measured at low frequencies, we should identify the form of transfer function(s) that would produce the overall lag spectra.

It is important to note that the lag spectra derive from the phases of the Fourier transform of the transfer function. The amplitude information is carried in the cross-band power spectrum,

¹ We note that the model is not a good fit to the data over the entire energy range, in particular there are significant residuals of 20 percent in the Fe K emission region, as seen in Fig. 8 of Z10, in addition to significant residuals below 5 keV that Z10 argue might be an effect of additional variations in ionisation. The extreme blurring in the model has erased features around Fe K that are present in the data. However, the Z10 model requires such extreme blurring, so we retain that model in our test.

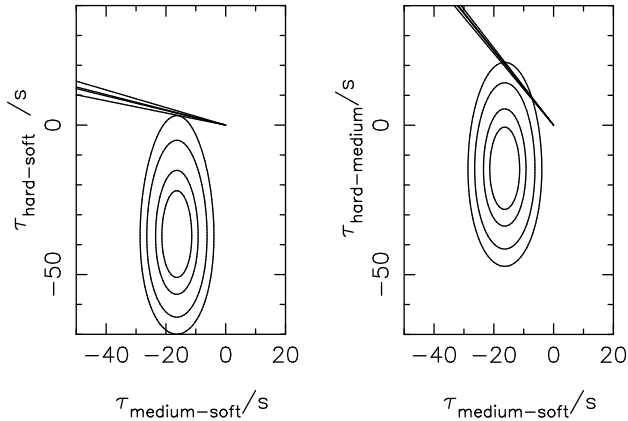


Figure 3. Confidence regions for the mean lags in the frequency range $0.00066 < \nu < 0.0053$ Hz between (left) hard-soft and medium-soft bands and (right) hard-medium and medium-soft bands. Contours are shown corresponding to the 68%, 90%, 99% and 99.9% confidence regions. Straight lines indicate the relationship between the lags in these bands expected from the Z10 model for each of the four O4 observations (only negative medium-soft lags are allowed in the Z10 model).

but it is mixed in with the unknown underlying cross-band spectrum, and so we have to rely on the phase information alone to inform us about the transfer function. Thus we cannot uniquely create a transfer function from the lag information. We can however consider some simple models that may have some link to physical reality and that create the observed lag spectrum features.

There are three effects that could lead to lag spectra of the form seen in Fig. 2. First, transfer functions with sharp transitions in general have oscillatory phases, and if the transfer function has a maximum away from zero lag, the phase oscillations can go negative. Such transfer functions may be generated by clumpy reverberating material or material not isotropically surrounding the source (Miller et al. 2010). As an example, consider a transfer function that is a top hat in time delay, of width Δt centred on delay t_0 and with intensity some fraction f of the directly-viewed intensity. The lag spectrum, $\tau(\omega)$ for angular frequency ω , is given by

$$\tan \omega \tau = \frac{f \text{sinc}(\omega \Delta t / 2) \sin \omega t_0}{1 + f \text{sinc}(\omega \Delta t / 2) \cos \omega t_0} \quad (3)$$

An example is shown in Fig. 4a for $\Delta t = t_0 = 1000$ s, $f = 1$. Negative time lags are seen at high frequencies, although it is difficult to obtain negative lags over a wide frequency range from reverberation in one band only. However, in section 4.1 (iv) we noted that reverberation is likely to be present at differing levels in both bands being cross-correlated. Fig. 4b shows the lag spectrum expected for transfer functions that are uniform from delay $t = 0$ to t_1 where $t_1 = 1000$ and 200 s in each of two bands, and with reflection fractions $f = 1$ and 0.5. Now a broader range of negative frequencies is seen. Finally we consider the effect of the transfer functions having no reflection less than some cutoff: Fig. 4c shows the same transfer functions as (b) but with no reflection at delays $t < 100$ s. This allows additional positive oscillations at high frequencies.

We can approximately fit this simple top-hat model to the measurements (Fig. 2). The models shown were fitted jointly to the three lag spectra in two stages. For speed, an initial fitting procedure minimised χ^2 ignoring the covariance between parameters and the non-independence of the lag spectra. Because the lag uncertainties are non-gaussian, and because there is covariance between both lag values and cross-band power spectrum amplitudes, to es-

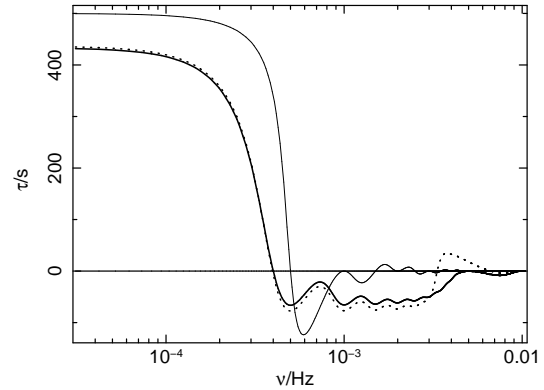


Figure 4. Models illustrating oscillatory lag spectra: (a) *thin solid line* top-hat transfer function in one band only; (b) *thick solid line* top-hat transfer functions in two bands, both transfer functions continuous from zero lag; (c) *dotted line* as (b) but with no reflection delays shorter than 100 s (see text for details).

timate the goodness-of-fit we then took this model and refitted the time series using the maximum likelihood method, but with time lags fixed to the model values. From this, the goodness-of-fit was evaluated as $\chi^2 = -2 \log(\mathcal{L}/\mathcal{L}_{\max})$ where \mathcal{L} was the model likelihood and \mathcal{L}_{\max} was the maximum likelihood found by allowing each frequency bin to have an independent time lag (i.e. the values shown as discrete values in Fig. 2). Considering just the hard-soft and medium-soft lags, to avoid the problem that all three lag spectra are not statistically independent, the model shown had $\chi^2 = 23$ for 25 degrees of freedom, a statistically-acceptable fit. The model fitted is one of the simplest possible models that we could have chosen, and the key point of this exercise is that even this simple model generates well the large positive lags at low frequencies, the sharp transition, and the extended range of high frequencies over which the lags appear small but negative. No such model has been demonstrated for the inner-disk reflection hypothesis of F09/Z10, which was ruled out by the considerations of section 4.2.2.

The best-fit top-hat start time was 100 s, assumed common to all three bands. The maximum time delays for the hard, medium and soft bands were 1800, 1450 and 150 s respectively, and the ratios f of flux in the reflected component to flux in the directly-viewed component (which may itself be partially obscured) were 0.67, 0.38 and 0.30 respectively. We do not evaluate uncertainties on these parameter values as this is computationally extremely expensive, requiring stepping through all parameter values and re-maximising the likelihood in the time domain, and the model is almost certainly too simple to be taken too literally. However, the values do indicate a possible physical origin for the different transfer functions in the three bands. The maximum time delay increases with energy: this is expected if X-rays are scattered while travelling through a medium whose opacity decreases with increasing energy, because then in the soft band X-ray photons cannot travel far through the medium before being absorbed, and any scattered X-rays must have relatively short time delays, whereas hard X-ray photons can travel further and create reverberation signals with longer delays. In this case we would expect also to see a greater fraction of scattered X-rays in the hard band, qualitatively in agreement with the inferred fractions. However, the observed fractions are also affected by any absorption of the directly-seen radiation, which cannot be determined from this analysis, and the predicted fraction of scattered light depends on the unknown radial distribution of scattering and absorbing material, making a more quantita-

tive test difficult to achieve. This inference implies that the reverberation transfer functions appear to arise from reflection or scattering from a distribution of material rather than from an unobscured reflector such as a naked accretion disk. Given the high fractions of reflected light, we infer that either the reverberating material subtends a large solid angle at the source, or that the directly-viewed emission is partially-obscured, or both.

According to this simple model, the reverberation in the soft band is characterised primarily by small delays, $100 \lesssim \tau \lesssim 150$ s. However, as noted in section 4.1, the existence of small lags cannot be taken as evidence for a short light travel time between source and reflector. In the case of 1H0707–495, the model is only viable if the medium and hard bands have time delays up to approximately 1800 s. Thus, even if one wished to assert that the soft-band reverberation were caused by inner-disk reflection, one would require the medium and hard band reverberation to be produced at significantly larger distances, with no physical explanation for that difference. Such an explanation would not allow models with these transfer functions in which both soft-band Fe L and hard-band Fe K emission were reflected from the same inner disk region.

4.4 Spectral modelling and further work

The aim of this letter has been to investigate the timing information for 1H0707–495 rather than to address the spectral model. The above analysis strongly indicates that there is a substantial component of scattered light present in the spectrum. Spectral modelling of this source to date has only considered either extreme relativistically-blurred models with little obscuration (F09, Z10) or partially-covering absorption models (Gallo et al. 2004) with no scattering. Z10 claim to have ruled out the partial covering models based on the weak observed strength of Fe K α emission, but we note that their argument has already been discounted by Miller et al. (2009) and Yaqoob et al. (2010). In fact, both sets of published models require unattractively high values of Fe abundance, around 11 for the relativistically-blurred model (F09) and around 3 for the partial-covering model (Gallo et al. 2004). The indication that there is a substantial fraction of X-rays scattered on passing through an absorbing medium means that models that include both absorption and scattering are required. The smooth spectral features in the soft band indicate that the scattered emission is likely to be smoothed by Compton scattering as seen in the Monte-Carlo radiative transfer models of transmission through a disk wind of Sim et al. (2008, 2010a,b), and the presence of a large amount of scattered light provides a natural way of obtaining a high equivalent width in a broad, smooth emission feature, which is likely combined with strong absorption edges. Further modelling such as that of Sim et al. (op. cit.) is required to make progress.

5 CONCLUSIONS

We have measured and analysed the time lags in 1H0707–495 between three X-ray bands: the soft (0.3–1 keV) and medium (1–4 keV) bands discussed by F09 and Z10, and the hard band (4–7.5 keV) not previously considered by those authors. Time lags have been analysed in the Fourier domain. We can summarise our conclusions as follows.

(i) The F09/Z10 model requires separate mechanisms for the positive lags at low frequencies and the negative lags at high frequencies, and in Section 4.2.1 we have argued that this imposes

some special constraints on those mechanisms which may not be fulfilled in practice.

(ii) Consideration of the lags in all bands, soft, medium and hard, rules out models in which the inner accretion disk makes a significant contribution at both Fe L and Fe K energies, and thus rules out the spectral model of F09/Z10. In particular, the lags between the hard and medium bands and between the hard and soft bands are also negative in the same range of frequencies that the lags between medium and soft band are negative. Comparison between the observed lags and the lags predicted from the spectral model rules out the Z10 model at confidence > 99.9 percent.

(iii) A simple model of reverberation, in which all X-ray bands have differing levels of reverberation, provides a good quantitative description of the large positive lags at low frequencies and the high frequency transition to negative lags, and fits the full lag spectra between all bands given the measurement uncertainties.

(iv) The harder X-ray bands appear to require longer maximum time lags than softer bands, consistent with a geometry in which reverberation arises, not as reflection from a naked accretion disk, but from scattering of radiation that is passing through partially-opaque material. Time delays at least as large as 1800 s are required, placing a lower limit on the extent of the reverberating region of approximately 1000 light-seconds, corresponding to 20–100 gravitational radii for black hole mass in the range $10^7 M_\odot$ (Leighly 2004) to $2 \times 10^6 M_\odot$ (Z10, Zhou & Wang 2005) respectively.

(v) Spectral models that include the effects of both absorption and Compton scattering are required.

These results strengthen previous conclusions that X-ray observations of the inner regions of type-I AGN may be dominated by the effects of circumnuclear material a few light-hours from the central source (e.g. Miller et al. 2008; Risaliti et al. 2009; Miller et al. 2010). The material causes both scattering and absorption, and subtends a large solid angle at the source but with an anisotropic geometry. Coupled with the evidence for energetic outflows (e.g. Pounds & Reeves 2009; Reeves et al. 2009) it is likely that the reverberating material is associated with an accretion disk wind.

Acknowledgments. TJT acknowledges NASA grant NNX08AJ41G. Observations were obtained with *XMM-Newton*, an ESA science mission with instruments and contributions directly funded by ESA Member States and NASA. This research has made use of data obtained from the High Energy Astrophysics Science Archive Research Center (HEASARC), provided by NASA's Goddard Space Flight Center.

REFERENCES

- Arévalo P., Uttley P., 2006, MNRAS, 367, 801
- Boller T., Fabian A. C., Sunyaev R., Trümper J., Vaughan S., Balantyne D. R., Brandt W. N., Keil R., Iwasawa K., 2002, MNRAS, 329, L1
- Bond J. R., Jaffe A. H., Knox L., 1998, Phys. Rev. D, 57, 2117
- Fabian A. C., Miniutti G., Gallo L., Boller T., Tanaka Y., Vaughan S., Ross R. R., 2004, MNRAS, 353, 1071
- Fabian A. C., Zoghbi A., Ross R. R., Uttley P., Gallo L. C., Brandt W. N., Blustin A. J., Boller T., Caballero-Garcia M. D., Larsson J., Miller J. M., Miniutti G., Ponti G., Reis R. C., Reynolds C. S., Tanaka Y., Young A. J., 2009, Nature, 459, 540 (F09)
- Gallo L. C., Tanaka Y., Boller T., Fabian A. C., Vaughan S., Brandt W. N., 2004, MNRAS, 353, 1064
- Leighly K. M., 2004, ApJ, 611, 125

- Lumb D. H., Warwick R. S., Page M., De Luca A., 2002, *A&A*, 389, 93
- McHardy I. M., Arévalo P., Uttley P., Papadakis I. E., Summons D. P., Brinkmann W., Page M. J., 2007, *MNRAS*, 382, 985
- McHardy I. M., Papadakis I. E., Uttley P., Page M. J., Mason K. O., 2004, *MNRAS*, 348, 783
- Miller L., Turner T. J., Reeves J. N., 2008, *A&A*, 483, 437
- Miller L., Turner T. J., Reeves J. N., 2009, *MNRAS*, 399, L69
- Miller L., Turner T. J., Reeves J. N., Lobban A., Kraemer S. B., Crenshaw D. M., 2010, *MNRAS*, 403, 196
- Nowak M. A., Vaughan B. A., Wilms J., Dove J. B., Begelman M. C., 1999, *ApJ*, 510, 874
- Peterson B. M., 1993, *PASP*, 105, 247
- Pounds K. A., Reeves J. N., 2009, *MNRAS*, 397, 249
- Reeves J. N., O'Brien P. T., Braito V., Behar E., Miller L., Turner T. J., Fabian A. C., Kaspi S., Mushotzky R., Ward M., 2009, *ApJ*, 701, 493
- Risaliti G., Salvati M., Elvis M., Fabbiano G., Baldi A., Bianchi S., Braito V., Guainazzi M., Matt G., Miniutti G., Reeves J., Soria R., Zezas A., 2009, *MNRAS*, 393, L1
- Ross R. R., Fabian A. C., 2005, *MNRAS*, 358, 211
- Sim S. A., Long K. S., Miller L., Turner T. J., 2008, *MNRAS*, 388, 611
- Sim S. A., Miller L., Long K. S., Turner T. J., Reeves J. N., 2010a, *MNRAS*, 404, 1369
- Sim S. A., Proga D., Miller L., Long K. S., Turner T. J., 2010b, *MNRAS*, in press, preprint arXiv:1006.3449
- Tanaka Y., Bolter T., Gallo L., Keil R., Ueda Y., 2004, *PASJ*, 56, L9
- Uttley P., McHardy I. M., Papadakis I. E., 2002, *MNRAS*, 332, 231
- Yaqoob T., Murphy K. D., Miller L., Turner T. J., 2010, *MNRAS*, 401, 411
- Zhou X., Wang J., 2005, *ApJ*, 618, L83
- Zoghbi A., Fabian A. C., Uttley P., Miniutti G., Gallo L. C., Reynolds C. S., Miller J. M., Ponti G., 2010, *MNRAS*, 401, 2419 (Z10)